ISSN 1070-3284, Russian Journal of Coordination Chemistry, 2021, Vol. 47, No. 12, pp. 891–902. © Pleiades Publishing, Ltd., 2021.

Synthesis and Structural Characterization of Bioactive Ferrocenyl Substituted Hydrazones

S. Abbas[a], Imtiaz-ud-Din[a, *], M. Mehmood[a], A. Raheel[a], R. Ayub[b], M. Zahid[c], and M. N. Tahir[d]

[a] *Department of Chemistry, Quaid-i-Azam University, Islamabad, 45320 Pakistan*

[b] *RISE Processum AB, Bioeconomy and Health, Örnsköldsvik, 89122 Sweden*

[c] *Higher Education Department Govt. of the Punjab, Lahore, Pakistan*

[d] *Department of Physics, University of Sargodha, Sargodha, 40100 Pakistan*

**e-mail: drimtiazuddin@yahoo.com*

Received April 7, 2021; revised May 9, 2021; accepted May 15, 2021

Abstract—A series of ferrocenyl substituted hydrazones (**I**–**VII**) derived from ferrocene carboxaldehyde and substituted hydrazides have been prepared and characterized by FTIR, ^{1}H NMR spectroscopy, and crystallographic studies. The single-crystal X-ray analysis for **III**·0.5H_2O·0.5CH_3CN (CIF file CCDC no. 1968937) further authenticates the structural motif of the synthesized compounds. The C(11) of ferrocene carboxaldehyde is linked with N(1) of the hydrazide moiety with a bond length of 1.283(5) Å, confirming the binding of the two structural units present in the final product. They were preliminarily screened for their antimicrobial activity and demonstrate good results. The free radical scavenging activity for the compounds (**III**, **IV**) has been found to be more than 90% when compared with the ascorbic acid. The total antioxidant capacity and total reducing power assays for **VI** show significant activity whereas the data for the other compounds are also encouraging. Quantum chemical calculations at the DFT level predict that compound **II** is the softest while **VII** is the hardest within the series, resultantly **II** can be used as a synthon for further chemical reactions.

Keywords: ferrocene, hydrazones, DFT, X-ray structure, spectroscopy, antimicrobial

DOI: 10.1134/S107032842112006X

INTRODUCTION

Hydrazones, being vital species in heterocyclic chemistry, exhibit vast pharmacological activities [1–4]. They are considered significant compounds in bioactive regime covering clinical and biological applications [5–7] and are also associated in analytical chemistry as chelating agents and sensors [8, 9]. The functionality is considered to be linked with antimicrobial [10], antiplatelet [11–13], and antidiabetic [12] activities.

Ferrocene, being phenomenal in the field of medicinal organometallic chemistry [14, 15], engrossed the attention of researchers based on its unusual properties such as aromaticity, low toxicity, stability and redox activity, therefore, the core is an attractive pharmacophore in drug design [16, 17]. Considering the above mentioned structural aspects and in continuation to our previous research work [18–22], we report herein the design and synthesis of a new series of ferrocenyl substituted hydrazones with a few exceptions that have already been reported [23, 24]. In these structures, the ferrocene core is connected to heterocyclic and non-heterocyclic moieties through a hydrazine linkage. The synthesized compounds have also been bio-assayed for their possible antimicrobial as well as free radical scavenging activity besides the total antioxidant capacity (TAC) and the total reducing power (TRP) studies.

EXPERIMENTAL

Materials and methods. The hydrazides and ferrocene-carboxaldehyde are available commercially and were used as received. The organic and inorganic solvents of analytical grade were utilized in synthetic protocol. The melting point apparatus, model MP-D Mitamura Riken Kogyo Japan, was used to determine the melting points of newly synthesized compounds and are uncorrected. The IR spectrophotometer of model FTS 3000 MX was used to record IR spectra of the compounds as KBr discs. Bruker Advanced Digital 300 MHz FT-NMR spectrometer was used to record ^{1}H NMR spectra in deuterated solvents relative to Me_4Si. The METTLER TOLEDO Switzerland, model 823e was used to record the differential scanning calorimetry (DSC) curves.

Synthesis. The ferrocene containing hydrazones **I**–**VII** were carried out by reacting the stoichiometric amounts of ferroenecarboxaldehyde and the respective substituted hydrazide. The hydrazides were dis-

solved in dried ethanol followed by the addition of the respective aldehyde. The reaction mixture was refluxed for 6–7 h with constant stirring. The resultant solution was rotary evaporated to get the crude product which was recrystallized in acetonitrile–acetone mixture (3 : 1) to obtain the pure product and in some cases as crystalline substances.

Ferrocenyl-4-methylbenzohydrazone (L^1). Quantities used: 4-methylbenzhydrazide (0.150 g, 1 mmol), ferrocene carboxaldehyde (0.214 g, 1 mmol). Reddish brown powder, the yield was 60%; m.p. = 215°C.

FT-IR data (KBr; ν, cm^{-1}): 3213 ν(NH), 1633 ν(C=O), 1558 ν(C=N), 1118 ν(N–N), 485 ν(Cp–Fe–Cp); ^{1}H NMR data (300 MHz; DMSO; δ, ppm): 2.38 (CH_3), 8.3 (CH=N), 11.49 (NH), 7.32–7.82 (C–$H_{Aromatic}$), 4.23–4.46 (C–$H_{Ferrocene}$).

For $C_{19}H_{18}N_2OFe$ (M = 346.2)

Anal. calcd., %	C, 65.92	H, 5.24	N, 8.09
Found, %	C, 65.89	H, 5.20	N, 8.07

Ferrocenyl-3-hydroxy-2-naphthoicbenzoyl hydrazone (L^2). Quantities used: 3-hydroxy-2-naphthoic acid hydrazide (0.202 g, 1 mmol), ferrocenecarboxaldehyde (0.214 g, 1 mmol). Reddish brown powder; the yield was 65%; dec.= 148°C.

FT-IR data (KBr; ν, cm^{-1}): 3463 ν(NH), 1635 ν(C=O), 1546 ν(C=N), 1104 ν(N–N), 471 ν(Cp–Fe–Cp). ^{1}H NMR data (300 MHz; DMSO; δ, ppm): 11.78 (OH), 8.48 (CH=N), 11.49 (NH), 7.32–8.32 (C–$H_{Aromatic}$), 4.26–4.70 (C–$H_{Ferrocene}$).

For $C_{22}H_{18}N_2O_2Fe$ (M = 398.2)

Anal. calcd., %	C, 66.35	H, 4.56	N, 7.03
Found, %	C, 66.33	H, 4.57	N, 6.98

Ferrocenylnicotinicacid hydrazone (L^3). Quantities used: nicotinicacid hydrazide (0.685 g, 5 mmol), ferrocenecarboxaldehyde (0.750 g, 5 mmol). Red crystals, the yield was 67%; m.p. = 230°C.

FT-IR (KBr; ν, cm^{-1}): 3229 ν(NH), 1688 ν(C=O), 1556 ν(C=N), 1144 ν(N–N), 480 ν(Cp–Fe–Cp). ^{1}H NMR data (300 MHz; DMSO; δ, ppm): 9.06 (CH=N), 11.59 (NH), 7.21–7.93 (C–$H_{Aromatic}$), 4.22–4.71 (C–$H_{Ferrocene}$).

For $C_{17}H_{15}N_3OFe$ (M = 333.17)

Anal. calcd., %	C, 61.29	H, 4.54	N, 12.61
Found, %	C, 61.22	H, 4.52	N, 12.60

Ferrocenylisonicotinicacid hydrazone (L^4). Quantities used: isonicotinicacid hydrazide (0.137 g, 1 mmol), ferrocenecarboxaldehyde (0.214 g, 1 mmol). Chocolate brown powder, the yield was 60%; m.p. 236°C.

FT-IR data (KBr, ν, cm^{-1}): 3101 ν(NH), 1666 ν(C=O), 1549 ν(C=N), 1150 ν(N–N), 481 ν(Cp–Fe–Cp). ^{1}H NMR data (300 MHz; DMSO; δ, ppm): 8.77 (CH=N), 11.76 (NH), 7.66–8.78 (C–$H_{Aromatic}$), 4.25–4.68 (C–$H_{Ferrocene}$).

For $C_{17}H_{15}N_3OFe$ (M = 333.17)

Anal. calcd., %	C, 61.29	H, 4.54	N, 12.61
Found, %	C, 61.27	H, 4.55	N, 12.60

Ferrocenyl-4-hydroxybenzohydrazone (L^5). Quantities used: 4-hydroxybenzohydrazide (0.152 g, 1 mmol), ferrocenecarboxaldehyde (0.214 g, 1 mmol). Reddish crystals, the yield was 65%; m.p. = 250°C.

FT-IR data (KBr; ν, cm^{-1}): 3233 ν(NH), 1632 ν(C=O), 1549 ν(C=N), 1172 ν(N–N), 477 ν(Cp–Fe–Cp). ^{1}H NMR data (300 MHz; DMSO; δ, ppm): 11.53 (OH), 8.26 (CH=N), 10.09 (NH), 6.84–7.80 (C–$H_{Aromatic}$), 4.22–4.63 (C–$H_{Ferrocene}$).

For $C_{18}H_{16}N_2O_2Fe$ (M = 348.18)

Anal. calcd., %	C, 62.09	H, 4.63	N, 8.05
Found, %	C, 62.05	H, 4.60	N, 8.02

Ferrocenyl thiophenebenzohydrazone (L^6). Quantities used: thiophene-2-carboxylic acid hydrazide (0.142 g, 1 mmol), ferrocenecarboxaldehyde (0.214 g, 1 mmol). Reddish orange powder, the yield was 63%; dec. = 350°C.

FT-IR data (KBr; ν, cm^{-1}): 3080 ν(NH), 1631 ν(C=O), 1557 ν(C=N), 1105 ν(N–N), 482 ν(Cp–Fe–Cp). ^{1}H NMR data (300 MHz; DMSO; δ, ppm): 8.27 (CH=N), 11.59 (NH), 7.21–7.93 (C–$H_{Aromatic}$), 4.22–4.71 (C–$H_{Ferrocene}$).

For $C_{16}H_{14}N_2OSFe$ (M = 338.21)

Anal. calcd., %	C, 56.82	H, 4.17	N, 8.28
Found, %	C, 56.78	H, 4.16	N, 8.25

Ferrocenyl-4-methylbenzenesulfonohydrazone (L^7). Quantities used: 4-methylbenzenesulfonic acid hydrazide (0.186 g, 1 mmol), ferrocenecarboxaldehyde (0.214 g, 1 mmol). Black product, the yield was 60%; dec. = 184°C.

FT-IR data (KBr; ν, cm^{-1}): 3175 ν(NH), 1645 ν(C=O), 1609 ν(C=N), 1163 ν(N–N), 493 ν(Cp–Fe–Cp). ^{1}H NMR data (300 MHz; DMSO; δ, ppm): 2.21 (CH_3), 10.78 (NH), 7.06–7.67 (C–$H_{Aromatic}$), 4.23–4.42 (C–$H_{Ferrocene}$).

For $C_{18}H_{18}N_2O_2SFe$ (M = 382.26)

Anal. calcd., %	C, 56.56	H, 4.75	N, 7.33
Found, %	C, 56.53	H, 4.73	N, 7.32

X-ray crystallography. On a glass fiber, a red crystal was installed. The data was then compiled using a Bruker kappa APEXII CCD diffractometer [25]. The diffractometer was fitted with graphite monochromated MoK_α radiation (λ = 0.71073 Å). MULABS option in PLATON executes empirical absorption correction [26]. Lorentz and polarization effects were also taken into account when analyzing the data. All nonhydrogen atoms were anisotropically refined with SHELXL97, structural refinements were carried out with full matrix least squares on F^2 [27]. Table S1 summarizes the crystal data and collection information (as supporting information). Mercury software was used for molecular graphics [28].

Supplementary material for structure III·0.5H_2O·0.5CH_3CN has been deposited with the Cambridge Crystallographic Data Centre (CCDC no. 1968937; www.ccdc.cam.ac.uk/data_request/cif or by emailing data_ request@ccdc.cam.ac.uk).

Biological studies. *Antibacterial activity*. The bactericidal activity for the synthesized compounds were assessed by using disc diffusion method [29]. The bacterial culture of various strains were used to make agar plates, which are *Staphylococcus aureus* (ATCC-6538), *Bacillus subtilis* (ATCC-6633), *Escherichia coli* (ATCC-25922), *Klebsiella pneumoniae* (ATCC-1705), *Pseudomonas aeruginosa* (ATCC-15442). Each of the compound (5 μL from 20 mg/mL DMSO), standard (cefixime 5 μL from 4 mg/mL DMSO) and negative control (DMSO, 5 μL) was loaded on the agar plates. The samples were incubated for 24 h at 37°C and then average zone of inhibition was measured.

Antifungal activity. Antifungal potential of the synthesized compounds was investigated using agar disc diffusion method [24]. The fungal culture of various strains was used to make agar plates, which are *Fusarium solani* (FCBP-0291), *Aspergillus fumigatus* (FCBP-66), *Mucor* species (FCBP-0300) and *Aspergillus flavus* (FCBP-0064). The strains were then suspended in 0.02% Tween 20 solution. The 100 μL of each fungal strain was swabbed onto dextrose agar plates. Impregnation of sterile filter paper discs were done with 5 μL of the synthesized compound (20 mg/mL DMSO), DMSO (negative control) and clotrimazole (standard, 4 mg/mL DMSO). The zone of inhibition was documented after an incubation of 24–48 h at 28°C.

Free radical scavenging assay (FRSA). The synthesized compounds were also screened for FRSA using the standard procedure [30]. An aliquot of 20 μL from each of the compounds (2 mg/mL DMSO) was added to 180 μL of DPPH solution (9.20 mg/100 mL methanol) and mixed thoroughly. Afterward incubation was done at 37°C for 30 min, and finally the absorbance was measured at 515 nm and the results were computed as percentage.

Total antioxidant capacity. The TAC of the compounds was evaluated using phosphomolybdenum based assay [30]. A volume of 900 μL of the reagent (0.6 M sulphuric acid, 28 mM sodium phosphate and 4 mM ammonium molybdate) was mixed with 100 μL of the compound (2 mg/mL DMSO), whereas DMSO was used as a blank. This reaction mixture was incubated at 95°C for 90 min and finally absorbance was measured at 695 nm.

Total reducing power. The TRP values of the synthesized compounds were estimated by using potassium ferricyanide colorimetric assay with slight modifications [30]. An aliquot of 200 μL of each compound (2 mg/mL DMSO) was added into potassium ferricyanide (1% w/v in H_2O) and 400 μL phosphate buffer (0.2 mol/L, pH 6.6) solutions, then it was incubated for 20 min at 50°C. After pouring 400 μL of trichloroacetic acid (10% w/v in H_2O) into each of the test extract and the mixture was, then, centrifuged for 10 min at room temperature. The 500 μL of supernatant was separated and mixed with 500 μL distilled water and 100 μL of $FeCl_3$ (0.1% w/v in H_2O). The absorbance was measured at 700 nm and the PRP value was expressed as μg AAE/mg of the compound.

The quantum chemical calculations. The time-dependent density functional theory (TD-DFT) employed Gaussian 16 program package with revision B.01 for all quantum chemical (QC) calculations [29]. The standard density functional theory (DFT) was used for geometry optimizations. The DFT methods have relatively lower cost than ab-initio methods and the results are comparably accurate, therefore, they are chosen for investigating the electronic structure of compounds. Furthermore, calculations of the harmonic vibrational analytical frequencies confirmed that these structures are real minimum and displayed no imaginary frequencies ($N_{img} = 0$). All geometry optimizations were carried out in the gas phase. The TD-DFT was also used to study the properties of frontier molecular orbitals. In all the QC calculations, the B3LYP hybrid functional, Becki three-parameter exchange [30, 31] and Lee, Yang, and Parr correlation functional [30] were employed. The LANL2DZ basis set [32–34] was used for Fe atom while 6-311+G(d,p) basis set [35–37] was used for all other elements, C, H, O, N, and S. Geometry of all the molecules was fully optimized in the electronic ground state in the gas phase by using these split basis set 6-311+G(d,p)/LANL2DZ. Similarly, mixed basis set was also used for.

These computational approaches give insights into the detailed electronic structural information of molecules and optimize the energies, ionization energies (IE), electron affinities (EA), HOMO–LUMO energy gaps/band gap (ΔE), hardness (η), softness (σ), and electronegativity (χ). Following equations were employed to calculate the above-mentioned properties.

$$\Delta E = E_{LUMO} - E_{HOMO}, \quad (1)$$

$$IE(I) = -E_{HOMO}, \quad (2)$$

$$EA(A) = -E_{LUMO}, \quad (3)$$

$$\chi = (I + A)/2, \quad (4)$$

$$\eta = (I - A)/2, \quad (5)$$

$$\sigma = 1/\eta. \quad (6)$$

RESULTS AND DISCUSSION

Seven compounds **I**–**VII** were synthesized by condensation reaction between ferrocene carboxaldehyde and the respective hydrazides in mole ratio 1 : 1 as enunciated in Scheme 1. They are stable in moist air and are characterized by spectroscopic and single crystal XRD data in addition to DSC data and elemental analyses.

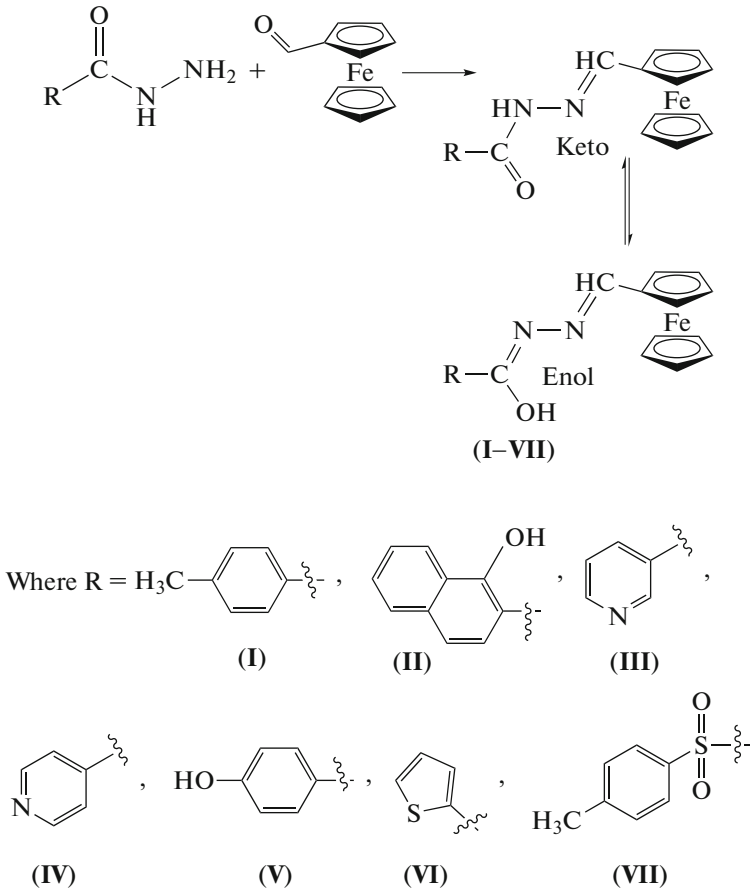

Scheme 1.

The FTIR data revealed the presence of all the functionality in the target compounds **I**–**VII**. The most prominent stretching vibrational band for C=N was observed in range 1609–1546 cm^{-1}. Another investigative absorption band, which defines the binding mode with the ferrocenyl moiety, is carbonyl stretch (C=O) that appeared in range 1631–1688 cm^{-1}. The absorption band for ferrocene moiety was observed around 480 cm^{-1} as reported earlier [15]. All the IR absorption bands give validity to the structural motifs of the target compounds. The FTIR spectra of the synthesized compounds are given as supplementary information (Figs. S1–S7).

The structures of all the synthesized ferrocenyl substituted hydrazones (**I**–**VII**) have been further elucidated by using ^1H NMR data which clearly described the existence of all the magnetically non-equivalent full stop after protons. The chemical shift values for various groups assist in determining the structural motifs that are present in the target compounds. The chemical shifts appeared in ranges 11.53–11.78, 10.78–11.90 and 8.26–9.06 ppm for OH, NH and CH functionality, respectively. The aromatic protons resonate in their usual region and the ferrocenyl protons resolved around 4.22–4.71 ppm in all the compounds as earlier reports manifested [14, 15]. All the chemical shift values validate the proposed chemical structure of the target compounds. The ^1H NMR spectra for the synthesized compounds are provided as supplementary information (Figs. S8–S14).

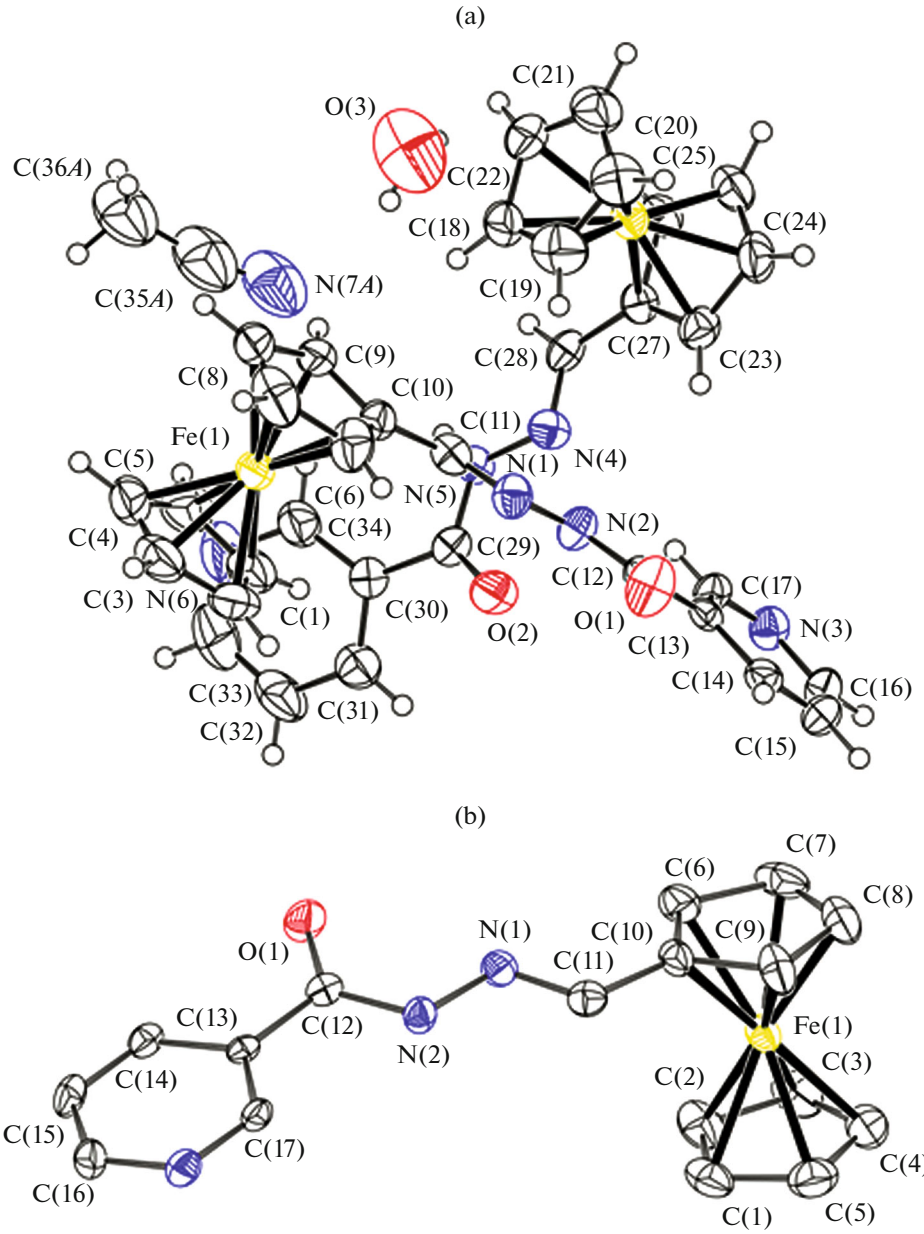

Fig. 1. ORTEP diagram for **III**·0.5H_2O·0.5CH_3CN (a) for single moiety drawn at 50% thermal ellipsoid level with atomic numbering scheme; (b) where H-atoms are removed for clarity.

The ORTEP diagram for **III**·0.5H_2O·0.5CH_3CN is delineated in Fig. 1a, whereas its structural refinement parameters and crystallographic data are presented in Table 1. The bond lengths and bond angles have been given in Tables 2 and 3, respectively. The compound crystallizes in monoclinic system with space group $P2_1/c$. The crystalline structure revealed that its single crystal comprises of two molecules and are solvated with acetonitrile and water molecules as depicted in Fig. 1a whereas Fig. 1b represents only one moiety of the twinned structure. Therefore, molecular formula for the compound may be designated as Fc–CH=N–NH–C(O)–Py-3·0.5H_2O·0.5CH_3CN (**III**·0.5H_2O·0.5CH_3CN). The packing diagram demonstrated the presence of four formula units per unit cell.

The compound **III** is a new one but shows some similarity to the structure that has already been reported by Tirkey et al. [38], but here Fc–CH=N–NH-moiety is present instead of Fc–C(CH_3)=N–NH– in the already reported structure whereas N of the pyridine functionality is at meta position in the presented structure instead of the reported para position. The compound reported here crystalizes out with acetonitrile and water molecules whereas the crystal structure reported by Tirkey, demonstrated only

Table 1. Crystallographic data and structure refinement for **III**·0.5H_2O·0.5CH_3CN

Parameter	Value
Empirical formula	$2(C_{17}H_{15}N_3OFe)\cdot CH_3CN\cdot H_2O$
Formula weight	725.41
Temperature, K	296(2)
Crystal system	Monoclinic
Space group	$P2_1/c$
a, Å	16.659(2)
b, Å	10.2546(10)
c, Å	21.063(2)
α, deg	90
β, deg	110.382(3)
γ, deg	90
Volume, Å^3	3373.0(7)
Z	4
ρ_{calcd}, g/cm^3	1.428
μ, mm^{-1}	0.907
F(000)	1504.0
Crystal size, mm	0.40 × 0.24 × 0.20
Radiation (λ, Å)	MoK_α (0.71073)
2θ Range for data collection, deg	4.752–52
Index ranges	$-20 \le h \le 20$, $-12 \le k \le 12$, $-25 \le l \le 25$
Reflections collected	12729
Independent reflections	6622 (R_{int} = 0.0812, R_{sigma} = 0.1457)
Data/restraints/parameters	6622/7/439
Goodness-of-fit on F^2	0.967
Final R indexes ($I \ge 2\sigma(I)$)	R_1 = 0.0636, wR_2 = 0.1132
Final R indexes (all data)	R_1 = 0.1263, wR_2 = 0.1309
Largest diff. peak/hole, e Å^{-3}	0.39/–0.45

Table 2. Selected bond lengths (Å) for complex **III**·5H_2O·0.5CH_3CN

Bond	d, Å	Bond	d, Å	Bond	d, Å
Fe(1)–C(1)	2.053(5)	Fe(1)–C(7)	2.045(5)	N(1)–C(11)	1.285(5)
Fe(1)–C(2)	2.041(4)	Fe(1)–C(8)	2.027(5)	N(2)–C(12)	1.356(5)
Fe(1)–C(3)	2.041(5)	Fe(1)–C(9)	2.027(4)	N(3)–C(16)	1.344(5)
Fe(1)–C(4)	2.047(5)	Fe(1)–C(10)	2.040(4)	N(3)–C(17)	1.324(5)
Fe(1)–C(5)	2.037(5)	O(1)–C(l2)	1.229(4)	C(1)–C(2)	1.413(6)
Fe(1)–C(6)	2.050(5)	N(1)–N(2)	1.376(5)	C(1)–C(5)	1.412(7)

Table 3. Selected angles (deg) for complex **III**·$5H_2O$·$0.5CH_3CN$

Angle	ω, deg	Angle	ω, deg	Angle	ω, deg
C(2)Fe(1)C(1)	40.37(18)	Cl(1)N(1)N(2)	115.9(4)	C(9)C(10)Fe(1)	68.8(2)
C(3)Fe(1)C(1)	67.8(2)	Cl(1)N(1)N(2)	119.4(3)	C(9)C(10)C(6)	108.2(4)
C(3)Fe(1)C(2)	40.22(19)	Cl(7)N(3)Cl(6)	118.2(4)	C(11)C(10)Fe(1)	124.9(3)
C(4)Fe(1)C(1)	68.1(2)	C(2)C(1)Fe	69.4(3)	C(11)C(10)C(6)	126.3(4)
C(4)Fe(1)C(2)	67.5(2)	C(5)C(1)Fe	69.2(3)	C(11)C(10)C(9)	125.5(4)
C(4)Fe(1)C(3)	39.76(19)	C(5)C(1)C(2)	106.3(5)	C(10)C(11)N(1)	121.2(4)

hydrated molecule. The C(11) of ferrocene carboxaldehyde is linked with N(1) of the hydrazide moiety with the bond length of 1.283(5) Å, which confirmed the binding of two structural moieties (ferrocene and hydrazide) in the final product. The bond distance between N(1) and N(2) is 1.376(4) Å which is shorter than the usual single bond indicating some double bond character, whereas the bond distance between C(11) and N(1) is 1.282(6) Å. Which is in agreement with the previously reported ferrocenyl Schiff bases [23, 25–27], such as [(η^5-C_5H_5)Fe{(η^5-C_5H_4)C(H)=NN(H)C(O)C_6H_4OH}] (1.284(3) Å), [(η^5-C_5H_5)-Fe{(η^5-C_5H_4)C(H)=NN(H)C(O)C_6H_5}] (1.277(4) Å), and [(η^5-C_5H_5)Fe{(η^5-C_5H_4)C(H)=NN(H)C(O)-C_6H_4N}] (1.291(4) Å). The bond angle for N(1)C(11)C(10) is 121.2°(4), another important geometric parameter, describing the linkage of the two moieties (C(10) of the ferrocene linked with N(1) of the hydrazide).

A strong intermolecular hydrogen bonding has been found for **III**·$0.5H_2O$·$0.5CH_3CN$. The hydrogen atom of the moiety, N(2)–H(2A) of the first molecule, interact through H-bonding to the two different electronegative atoms of second molecule, that is, carbonyl oxygen O(2) and the N(4) atom with bond distances of 2.34 and 2.56 Å, respectively. These distances clearly indicate that the bond between H(2) and O(2) is stronger than the bond between H(2) and N(4). The bond angle of N(2)H(2*A*)O(2) and N(2)H(2*A*)N(4) is 127.0° and 156.3°, respectively. The hydrogen atom of the water molecule, [O3(2)–H(3A)] formed H-bonds with carbonyl oxygen O(1) and N(1) atoms of the first molecule **III** with bond distances of 2.13 and 2.65 Å, respectively. The bond angle of O3(2)H(3*A*)O(1) and O3(2)H(3A)N(1) is 154.4° and 135.7°, respectively. The nonclassical type of intramolecular H-bonding (NH···Fe) has also been reported in [39]. The H-bonding for **III**·$0.5H_2O$·$0.5CH_3CN$ is delineated in Fig. 2 and the relevant data are the following:

D–H...A	D–H, Å	H–A, Å	D–A, Å	Angle DHA, deg
N(2)–H(2*A*)...O(2)	0.86	2.34	2.936(4)	127.0
N(2)–H(2*A*)...N(4)	0.86	2.56	3.362(4)	156.3

The thermal analytical techniques are useful to study the physical state as well as thermal stability of the target compounds. The DSC data have been collected for the selective compounds **I**, **III** to assess their thermal behavior. The DSC thermogram for **I** is given as supplementary information (Fig. S15). A sharp endothermic peak at 228°C (with onset at 226 and end set at 237°C) has been found for **III** while for **I** exhibited the sharp endothermic peak at 211°C (with onset at 205 and end set at 216°C) which may be ascribed to melting temperature of the respective compounds. The sharpness of the peaks indicates purity of the compounds. Moreover, they exhibit only one melting peak which demonstrates the absence of polymorphism. The compounds **I**, **III** exhibit broad exothermic peaks that described their decomposition pattern.

All the synthesized ferrocenyl hydrazones (**I–VII**) were evaluated for their possible bactericidal activity. For that, the samples were dissolved in DMSO and screened against two gram-positive (*B. subtilis* (ATCC-6633), *S. aureus* (ATCC-6538), and three gram negative-bacterial strains (*P. aeruginosa* (ATCC-15442), *K. pneumonia* (ATCC-1705) and *E. coli* (ATCC-25922). Most of the ferrocene substituted hydrazones exhibit considerable activity against gram positive strains, whereas compounds (**I–III**, **V** and **VII)** revealed good to moderate activity against *S. aureus* and *E. coli*. The minimum inhibitory concentration for all the synthesized ferrocenyl hydrazones is 100 μg/mL. Substituents on the hydrazide moiety affect the bactericidal efficacy of the derivatives having ferrocene core [40]. The presence of heteroatom in the compounds further increase their lipophilic character and help to enhancing the electrostatic affinity of the compounds by entering the

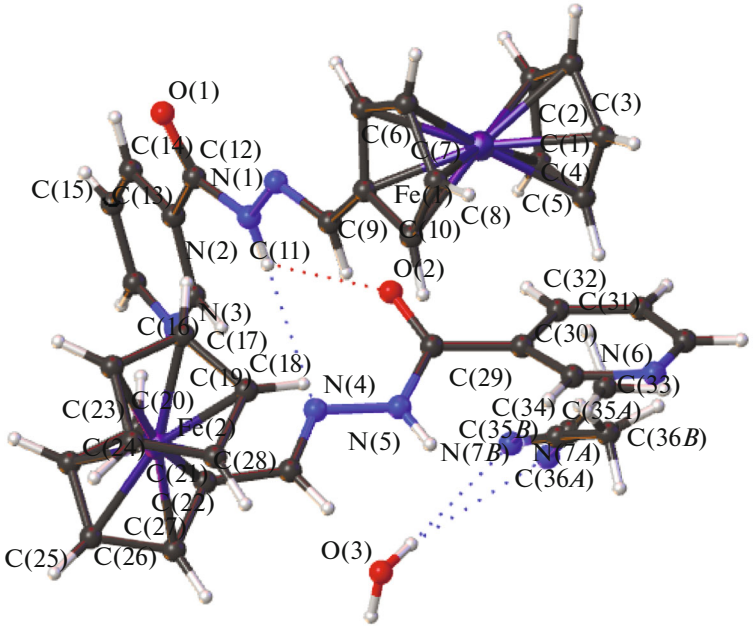

Fig. 2. Hydrogen bonding diagram for **III**·0.5H_2O·0.5CH_3CN.

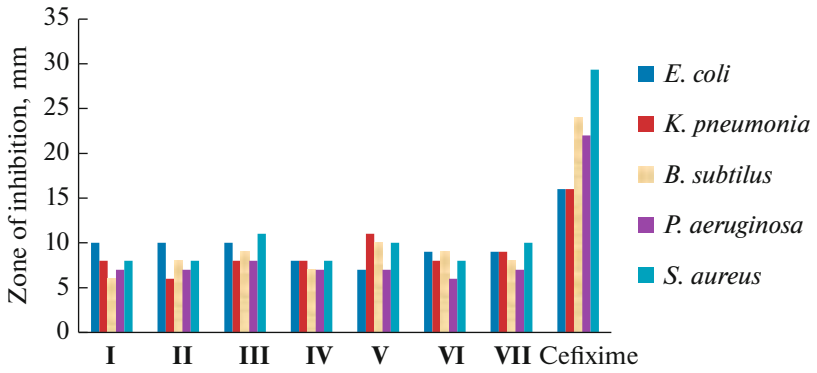

Fig. 3. Antibacterial activity for **I**–**VII**.

bacteria through lipo-polysaccharide sheath of cell wall. The synthesized compounds were also evaluated with respect to their fungicidal potential against *Mucor* (FCBP-0300), *F. solani* (FCBP-434), *A. fumigatus* (FCBP-66) and *A. flavus* (FCBP-0064). The data demonstrate that compounds (**I**, **V** and **VI**) exhibit very good antifungal potential against *Mucor*, *A. fumigatus* and *F. solani,* respectively. The target products are known to have less toxicity as compare to parent hydrazides, that might be attributed to the blocking of free entry of amino groups into the living species [41]. The antibacterial and antifungal activity data for the compounds have been provided in Tables S1 and S2, respectively, as supplementary information whereas the graphical presentations for antibacterial and antifungal activity have been delineated in Figs. 3 and 4, respectively.

The graphical representation for free radical scavenging activity for the target compounds **I**–**VII** is given in Fig. 5 and the data have been provided in Table S3 as supplementary information. The hydrazones showed supportive results vis-a-vis percentage free radical scavenging activity. The ferrocenyl nicotinic acid hydrazone (**III**) and ferrocenyl iso-nicotinic acid hydrazone (**IV**) revealed significant scavenging ability and have more than 90% activity which is comparable to the positive control (ascorbic acid). It may be argued that pyridyl containing ferrocenyl hydrazones exhibit high percent scavenging activity as they contain nitrogen in the ring, being electron donor in nature, it may stabilize the DPPH free radicals more effectively.

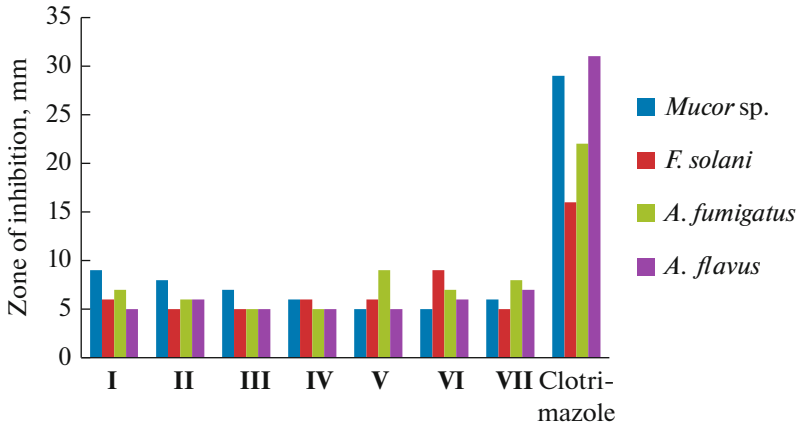

Fig. 4. Antifungal activity for **I–VII**.

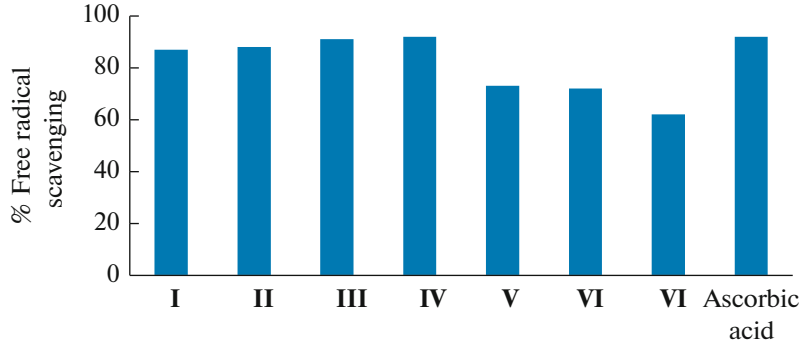

Fig. 5. % Free radical scavenging for **I–VII**.

The compounds **I–VII** were also explored with respect to their antioxidant capacity and reducing power, the data are quite significant (Table S4) and the graphical representation is given in Fig. 6. The structures possess conjugated aromatic system as well as the ferrocene moiety, the main contributors for the enhancement of their antioxidant capacity and reducing power as they dispense single electron on the whole molecule. The data manifest that the compounds may serve as potent antioxidants for future drug designing processes in the treatment of reactive oxygen species-induced diseases [42].

The quantum calculation data have been summarized in Table 4. The molecular properties like reactivity and stability of the compounds depend on their electronic structure and for that studies on HOMO and LUMO are conducted. Mostly oxidation (removal of an electron from HOMO) and reduction (addition of an electron to LUMO) depend on the energies of these two orbitals, therefore, it is important to predict such properties of the compounds. Here different electronic parameters were evaluated to investigate the reactivity and stability of ferrocenyl hydrazones **I–VII**. The results are also compared with the unsubstituted ferrocene molecule. Regarding frontier molecular orbitals, HOMO is located on the ferrocenyl part of the molecule and LUMO on the other terminal, the hydrazide side which has aromatic substituents. All the compounds follow the same trends in displaying their Frontier molecular orbitals (Fig. 7)

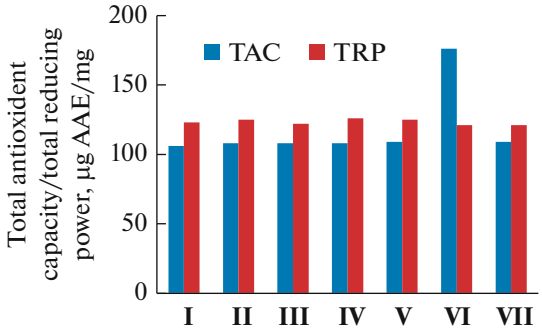

Fig. 6. Total antioxidant capacity and total reducing power for **I–VII**.

Table 4. The quantum chemical calculations data for **I**–**VII**, obtained at B3LYP/LANL2DZ-6-311+G(d,P) level

Compound	ΔE, eV	I ($-E_{HOMO}$), eV	A ($-E_{LUMO}$), eV	χ	H	σ	M, Debye
I	3.99	5.61	1.61	3.61	1.99	0.50	2.40
II	3.54	5.52	1.99	3.76	1.77	0.57	4.08
III	3.78	6.73	1.96	3.84	1.89	0.53	1.29
IV	3.65	5.78	2.13	3.96	1.82	0.55	2.51
V	4.06	5.61	1.55	3.58	2.03	0.49	3.12
VI	3.75	5.65	1.90	3.78	1.87	0.53	2.34
VII	4.12	5.95	1.83	3.89	2.06	0.49	7.83
Ferrocene	5.18	5.59	0.41	2.99	2.59	0.39	0.00

and showed complete delocalization across the entire molecule. The results of Mulliken charge distribution showed the sites of positive and negative charges and give an illustration of where the negative and positive sides are in the molecule and how electrons can flow from negative to the positive site. Unsubstituted ferrocene molecule has very high band gap of 5.18 eV in comparison to its hydrazone derivatives, having the values of about 3.54–4.12 eV. Different substituents, on the terminal side of the hydrazide, have significant impact on the electronic structure of these hydrazones. For example, the lowest band gap has been observed for **II** which has 1-naphthol as a substituent whereas highest band gap was observed for **VII**. The band gap energies decrease in the following order: ferrocene > **VII** > **V** > **I** > **III** > **VI** > **IV** > **II**.

Ferrocene displayed lowest values vis-a-vis electronegativity, electron affinity, and ionization energy within the reported series of compounds, whereas substitution on the hydrazide part of these hydrazones' derivatives may reduce/enhance these properties significantly owing to influence of conjugation and aromaticity within the framework. Moreover, compound **III** showed highest ionization energy whereas highest electron affinity and electronegativity values have been observed for **IV**. The values of hardness (η) appeared in range 1.77–2.59 and the compound **VII** exhibits the hardest character within the series. Regarding softness (σ) characteristics, the values are in range 0.39–0.57, describing that **II** is the softest and **VII** is the least soft compound among the synthesized products. In other words, **VII** has been observed to be

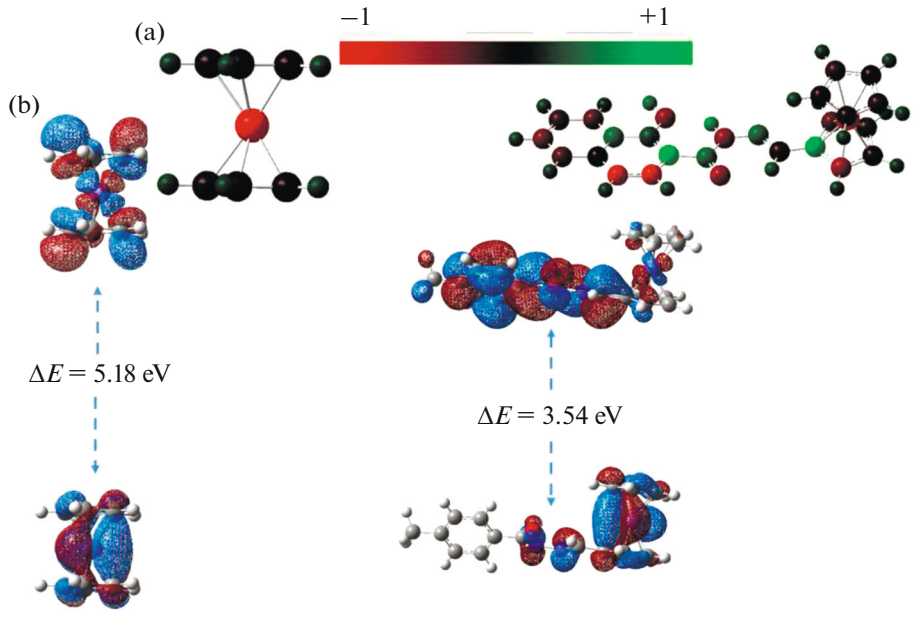

Fig. 7. Mullikan charge density (a) and molecular orbitals (iso-surface: 0.02) with band gap (ΔE) of ferrocene (left) and compound (**II**) (right) (b). Red color indicates sites of negative charge and green color indicates sites of positive charge in Mullikan charge density plots.

the hardest, while **II** displayed high softness within the series and vice versa. The outcome of the study is that the compound **II** is a favorable entity for further synthetic reactions, possibly due to the presence of –OH substituent on the naphthalene moiety. It has been argued that hard compounds are more resistant towards chemical reactions in comparison to the softer ones because of increased deformation of electronic cloud. The values of dipole moments have also been determined for the compounds and are found in range 0.0–7.83 D. The data show that **III** is the least polar compound whereas **VII** is the highly polar species within the series.

Thus, results of DFT studies provide mechanistic interpretation of various experimental properties of the compounds which may help in designing new chemical reactions. It is anticipated that similar strategies may be applied before designing further chemical reactions in future research endeavors.

CONCLUSIONS

Seven Schiff base hydrazones **I**–**VII** containing ferrocenyl core have been synthesized and characterized by spectroscopy and single crystal X-ray analysis. The structures of some new compounds have also been compared with the already synthesized ones and found good structural correlation among them. Sometimes these types of studies have to be done to further explore their biological and non-biological properties. They were preliminary screened for their antimicrobial activity and found good results. The compounds **III** and **IV** exhibit excellent free radical scavenging activity when compared to ascorbic acid, using as a standard. The total antioxidant capacity and total reducing power assay data for some of the compounds provide a fundamental outline for drug discovery process and need to be further explored in this regard. The results of QC calculations such as DFT indicated that the electronic properties of ferrocene can be modified/tuned by making its hydrazone derivatives. It has been observed that **II** has the lowest HOMO–LUMO gap, lowest ionization energy, softer and least hard within the reported compounds. Thus, compound **II** can serve as an important synthon for designing futuristic chemical reactions.

ACKNOWLEDGMENTS

The authors are thankful to HEC, Pakistan, and Quaid-i-Azam University for their financial support. The computations were enabled by resources provided by the Swedish National Infrastructure for Computing (SNIC) and Uppsala Multidisciplinary Center for Advanced Computational Science (UPPMAX) at the National Supercomputer Center (NSC), Linköping under the projects SNIC 2020/13-45 and SNIC 2020/15-195.

CONFLICT OF INTEREST

The authors declare that they have no conflicts of interest.

SUPPLEMENTARY MATERIALS

The online version contains supplementary material available at https://doi.org/10.1134/S107032842112006X.

REFERENCES

1. Gao, P. and Wei, Y., *Heterocycl. Commun.*, 2013, vol. 19, p. 113.
2. Rao, A.B. and Pal, S., *J. Organomet. Chem.*, 2013, vol. 731, p. 67.
3. Chen, K., Hu, Y., Li, Q.-S., et al., *Bioorg. Med. Chem.*, 2012, vol. 20, p. 903.
4. Jacobsen, N., *Angew. Chem. Int. Ed.*, 2007, vol. 46, p. 1315.
5. Verma, G., Marella, A., Shaquiquzzaman, M., et al., *J. Pharm. Bioall. Sci.*, 2014, vol. 6, p. 69.
6. Verma, G., Marella, A., Shaquiquzzaman, M., et al., *J. Pharm. Bioall. Sci.*, 2014, vol. 6, p. 69.
7. Singh, N., Ranjana, R., Kumari, M., and Kumar, B., *Int. J. Pharm. Clin. Res.*, 2016, vol. 8, p. 162.
8. Fournand, D., Arnaud, A., and Galzy, P., *J. Mol. Catal., B*, 1998, vol. 4, p. 77.
9. Arivazhagan, C., Borthakur, R., and Ghosh, S., *Organometallics*, 2015, vol. 34, p. 1147.
10. Özkay, Y., Tunalı, Y., Karaca, H., and Işıkdağ, İ., *Eur. J. Med. Chem.*, 2010, vol. 45, p. 3293.
11. Mashayekhi, V., Tehrani, K.H.M.E., Amidi, S., and Kobarfard, F., *Chem. Pharm. Bull.*, 2012, c12-00597.
12. Todeschini, A.R., de Miranda, A.L.P., da Silva, K.C.M., et al., *Eur. J. Med. Chem.*, 1998, vol. 33, p. 189.
13. Tehrani, K.H.M.E., Zadeh, M.E., Mashayekhi, V., et al., *Iran J. Pharm. Res.*, 2015, vol. 14, p. 1077.
14. Hartingerand, C.G. and Dyson, P.J., *Chem. Soc. Rev.*, 2009, vol. 38, p. 391.
15. Sansook, S., Hassell-Hart, S., Ocasio, C., and Spencer, J., *J. Organomet. Chem.*, 2019, p. 121017.
16. Chavain, N. and Biot, C., *Curr. Med. Chem.*, 2010, vol. 17, p. 2729.
17. Hillard, E., Vessières, A., Thouin, L., et al., *Angew. Chem. Int. Ed.*, 2006, vol. 45, p. 285. https://doi.org/10.1002/anie.200502925
18. Tehseen Fatima, Imtiaz-ud-Din, Ali Akbar, Muhammad Sabieh Anwar, and Muhammad Nawaz Tahir, *J. Mol. Struct.*, 2019, vol. 1184, p. 462. https://doi.org/10.1016/j.molstruc.2019.02.037
19. Raheel, A., Imtiaz-ud-Din, Andleeb, S., et al., *Appl. Organomet. Chem.*, 2017, vol. 31, e3632. https://doi.org/10.1002/aoc.3632
20. Andleeb, S. and Imtiaz-ud-Din, *J. Organomet. Chem.*, 2019, article 120871. https://doi.org/10.1016/j.jorganchem.2019.120871
21. Din Imtiaz ud, Mazhar, M., Molloy, K.C, and Khan, K.M., *J. Organomet. Chem.*, 2006, vol. 691,

p. 1643.
https://doi.org/10.1016/j.jorganchem.2005.12.013

22. Sumaira Abbas, Imtiaz-ud-Din Din, Ahmad Raheel, and Asim Tameez ud Din, *Appl. Organomet. Chem.*, 2020, vol. 34, e5413.
https://doi.org/10.1002/aoc.5413
23. Mishra, S., Dewangan, S., Giri, S., et al., *Eur. J. Inorg. Chem.*, 2016, p. 5485.
24. Sathyadevi, P., Krishnamoorthy, P., Butorac, R.R., et al., *Metallomics*, 2012, vol. 4, p. 498.
25. *Bruker, APEX2, SAINT and SADABS*, Madison: Bruker AXS Inc., 2007.
26. Spek, A., *J. Appl. Crystallogr.*, 2003, vol. 36, p. 7.
27. Sheldrick, G.M., *SHELXS-97, Program for X-ray Crystal Structure Refinement*, Göttingen: Univ. of Göttingen, 1997.
28. Bruno, I.J., Cole, J.C., Edgington, P.R., et al., *Acta Crystallogr., Sect. B: Struct. Sci.*, 2002, vol. 58, p. 389.
29. Frisch, M., Trucks, G., Schlegel, H., et al., *Gaussian 16, Revision B. 01*, Wallingford CT: Gaussian Inc., 2016.
30. Becke, A.D., *Phys. Rev., A*, 1988, vol. 38, p. 3098.
31. Lee, C., Yang, W., and Parr, R.G., *Phys. Rev. B: Condens. Matter Mater. Phys.*, 1988, vol. 37, p. 785.
32. Hay, P.J., and Wadt, W.R., *J. Chem. Phys.*, 1985, vol. 82, p. 270.
33. Wadt, W.R. and Hay, P.J., *J. Chem. Phys.*, 1985, vol. 82, p. 284.
34. Hay, P.J. and Wadt, W.R., *J. Chem. Phys.*, 1985, vol. 82, p. 299.
35. McLean, A. and Chandler, G., *J. Chem. Phys.*, 1980, vol. 72, p. 5639.
36. Krishnan, R., Binkley, J.S., Seeger, R., and Pople, J.A., *J. Chem. Phys.*, 1980, vol. 72, p. 50.
37. Clark, T., Chandrasekhar, J., Spitznagel, G.W., and Schleyer, P.V.R.J., *Comput. Chem.*, 1983, vol. 4, p. 294.
38. Tirkey, V., Mishra, S., Dash, H.R., et al., *J. Organomet. Chem.*, 2013, vol. 732, p. 122.
39. Veit, P., Prantl, E., Förster, C., and Heinze, K., *Organometallics*, 2016, vol. 35, p. 249.
40. Chohan, Z.H., Scozzafava, A., and Supuran, C.T., *Synth. React. Inorg.*, 2003, vol. 33, p. 241.
41. Chohan, Z.H., Pervez, H., Khan, K.M., et al., *Med. Chem.*, 2005, vol. 20, p. 81.
42. Khelef, A. and Lanez, T., *Der Pharma Chem.*, 2015, vol. 7, p. 318.